Revista Mexicana de Astronomía y Astrofísica, **60**, 99–111 (2024)

https://doi.org/10.22201/ia.01851101p.2024.60.01.07

THE FIRST MULTICOLOUR PHOTOMETRY OF THE V840 LYR CONTACT BINARY STAR

Mehmet Tanrıver[1,2], Raúl Michel[3], Ahmet Bulut[4,5], Héctor Aceves[3], and Ahmet Keskin[1]

Received May 16 2023; accepted November 2 2023

ABSTRACT

Light curves for the total-eclipsing binary system V840 Lyr in the V, R_c, and I_c bands are presented; these display the O'Connell effect. Analysis was performed with the `Phoebe031a` software revealing that V840 Lyr is a W-type contact binary with a degree of contact factor of $f = 15.1 \pm 5.6\%$, a mass ratio of $q = 0.4509 \pm 0.0705$, an inclination of $i = 86.7°$, and a temperature difference of ΔT = 45 K. An asymmetry in the light curves was modeled assuming a cool spot located on the secondary star. The period changes of the system are examined by combining our recently found times of light minima together with those in the literature. Absolute parameters were obtained as $M_1 = 0.74\mathrm{M}_\odot$, $M_2 = 0.34\mathrm{M}_\odot$, $R_1 = 0.74\mathrm{R}_\odot$, and $R_2 = 0.51\mathrm{R}_\odot$ from our photometric solutions, using some empirical relations. The long-term period increase and the contact configuration indicate that V840 Lyr will evolve into a fill-out overcontact binary.

RESUMEN

Presentamos curvas de luz V, R_c, e I_c para el sistema binario totalmente eclipsante V840 Lyr; las cuales manifiestan el efecto O'Connell. Se hace el análisis usando el paquete `Phoebe031a`; encontramos que V840 Lyr es una binaria de contacto tipo-W, con factor de contacto $f = 15.1 \pm 5.6\%$, razón de masa $q = 0.4509 \pm 0.0705$, una inclinación de $i = 86.7°$, y diferencia de temperatura de ΔT = 45 K. Modelamos una asimetría en las curvas de luz asumiendo un mancha fría ubicada en la estrella secundaria. Los cambios de período del sistema se examinaron combinando nuestros tiempos mínimos de luz en conjunto con los de la literatura. Los parámetros absolutos obtenidos $M_1 = 0.74\mathrm{M}_\odot$, $M_2 = 0.34\mathrm{M}_\odot$, $R_1 = 0.74\mathrm{R}_\odot$, y $R_2 = 0.51\mathrm{R}_\odot$ resultan de nuestras soluciones fotométricas y utilizando relaciones empíricas. El aumento del período a largo plazo y la configuración de contacto indican que V840 Lyr evolucionará hacia una binaria de sobrecontacto rellena.

Key Words: stars: binaries: eclipsing — stars: binaries: general — stars: individual: V840 Lyr

1. INTRODUCTION

Super Wide Angle Search for Planets (SuperWASP), an international team of many academic institutions conducting an ultra-wide angle search for exoplanets using transit photometry, discovered that V840 Lyr (1SWASP J183738.17+402427.2 = 2MASS J18373818+4024271) is an eclipsing binary star with a short period (Norton et al. 2011). In the General Catalogue of Variable Stars (GCVS) database, V840 Lyr was identified by Samus et al. (2017) to be an eclipsing W UMa (EW) type binary. The system's ephemeris (***H***eliocentric ***J***ulian ***D***ay-HJD) was provided by (GCVS) database (Samus et al. 2017):

$$Min.I(HJD) = 2457423.1706 + 0.221311 \times E. \quad (1)$$

New high-quality photometric observations were made in order to study this binary. The multicolor light curves of the system demonstrated an O'Connell effect in the V, R_c, and I_c filters (see Figure 4). If the magnitude of the maximum-I is lower than that of the maximum-II, this is accepted as a positive O'Connell effect (O'Connell 1951).

[1]Department of Astronomy and Space Science, University of Erciyes, Türkiye (corresponding author: mtanriver@erciyes.edu.tr).
[2]Astronomy and Space Science Observatory Application and Research Center, University of Erciyes, Türkiye.
[3]Instituto de Astronomía, UNAM. Ensenada, México.
[4]Department of Physics, University of Çanakkale Onsekiz Mart, Türkiye.
[5]Astrophysics Research Centre and Observatory, University of Çanakkale Onsekiz Mart, Türkiye.

TABLE 1

THE TARGET STARS' COORDINATES

Target	Stars	R.A.(2000) h:m:s	DEC.(2000) ° ′ ″	V mag	Ref
C1	V840 Lyr	18:37:38.18	40:24:27.09	14.45	(1)
C2	Comparison	18:37:27.01	40:24:56.88	12.63	(2)
C3	Comparison	18:37:25.32	40:26:03.59	13.19	(2)
C4	Comparison	18:37:34.49	40:24:44.78	14.89	(2)
C5	Comparison	18:37:47.46	40:25:29.24	14.47	(2)
C6	Check	18:37:55.51	40:25:35.25	14.36	(2)

Ref: (1) SuperWASP (Norton et al. 2011); (2) CCD photometry.

The presence of a dark cool spot on the secondary star provided an explanation for the asymmetric light curves. Their photometric investigation revealed that the V840 Lyr is a W-type over-contact binary with a small mass ratio. The binary star's derived fill-out factor of 15.14 percent indicated that it is getting close to the end of its evolution. These characteristics suggest that V840 Lyr is a promising target for additional research, which is made in part in this work. When the binary system satisfies the well-known requirement that the orbital angular momentum is less than three times the total rotation angular momentum of the components ($J_{orb} < 3J_{rot}$), both components may merge into a rapidly spinning single star (Hut 1980). As a result, it is a potential progenitor for a luminous red nova (Zhu et al. 2016).

In this paper we study V840 Lyr further by analyzing light curves using a standard software package, and provide different estimates of the physical parameters for this binary star. Table 1 contains details on V840 Lyr, comparisons, and check stars. A typical binary of the EW type is V840 Lyr. The parallax for this eclipsing binary was stated as $\pi = 2.2235 \pm 0.0214$ mas in Gaia Data Release 2-3 (Gaia Collaboration; et al. 2018).

2. PHOTOMETRIC OBSERVATIONS

V, R_c and I_c observations were carried out with the Mexman filter wheel mounted on the 84 cm reflecting telescope at San Pedro Martir (SPM) Observatory during the nights of 2018 July 06 (2.6h), 2019 June 06 (0.9h), 2019 June 07 (3.2h) and 2021 September 27 (2.5h) using exposure times of 60s in V and 40s both in R_c and I_c. Additional observations where carried out in 2022 June 14 (2.3h) and 2022 June 17 (6.9h) with exposure times of 20s in V and 15s in both R_c and I_c. During the 2018 run the Spectral Instruments CCD camera was employed while the Marconi 5 camera was used during the other runs. Table 1 contains the coordinates of the variable (V840 Lyr), the comparisons and the check stars in the CCD camera's field of vision. The PHOT aperture photometry routine of IRAF was used for the reduction of the observed CCD field images.

The epoch specified in the GCVS, however, is ***H***eliocentric ***J***ulian ***D***ay-HJD (Samus et al. 2017), needs to be transformed to ***B***arycentric ***J***ulian ***D***ay-BJD to be compatible with TESS data. The following equation specifies the epoch as BJD:

$$BJD_{Min.I} = 2457423.0607315 + 0.221311 \times E. \quad (2)$$

To make this transformation, we used the code in the Eastman et al. (2010) study. Equation 2 specifies the epoch as BJD. In equation 2 period and epoch are taken from the GCVS catalog.

Table 2 lists the results of using the Gauss fitting method along with Monte Carlo Markov Chain (MCMC) to the following datasets: 14 CCD times of light minima from SPM observations, 18 from SWASP (Super Wide Angle Search for Planets (Pollacco et al. 2006), 3 from CRTS (Catalina Real-time Transient Survey, Drake et al. 2009), 9 from ZTF (The Zwicky Transient Facility (Bellm et al. 2019), and 10 from TESS (the Transiting Exoplanet Survey Satellite (Sullivan et al. 2015).

3. INVESTIGATION OF THE O-C CHANGE

Since the variable's discovery, no period change studies have been undertaken. We gather all available photoelectric and CCD times of minimum light from the other works, websites, and other surveys (SWASP, CRTS, ZTF, TESS) to examine the variations in the orbital period. Table 2 contains a list of minimum times of all primary and secondary eclipses. The seventh column of Table 2 contains a list of the (O-C) values (***O***bserved times of light minima minus ***C***omputed times of light minima), which are plotted in the top panel of Figure 1 and are calculated by equation 2. In this figure, black-filled and empty circles signify data from the SPM Observatory, black-filled and empty diamonds indicate data obtained from TESS light curves, black-filled and empty squares refer to data from SWASP, black-filled and empty triangles indicate data obtained from ZTF, and the black plus and the black cross refer to data from CRTS.

The following ephemeris is provided by the (O-C) values' least-squares solution:

$$(O-C) = 1.33484(2) \times 10^{-03} + 2.10185(3) \times 10^{-07} E. \quad (3)$$

This ephemeris' linear term allows to calculate the new period and new initial minimum time. These minimum times of the binary system were used to calculate the revised orbital period, as provided by equation 4:

$$BJD(MinI) = 2457422.62012184 + 0.22131121 \times E \quad (\pm 0.00025736) \quad (\pm 0.00000002). \quad (4)$$

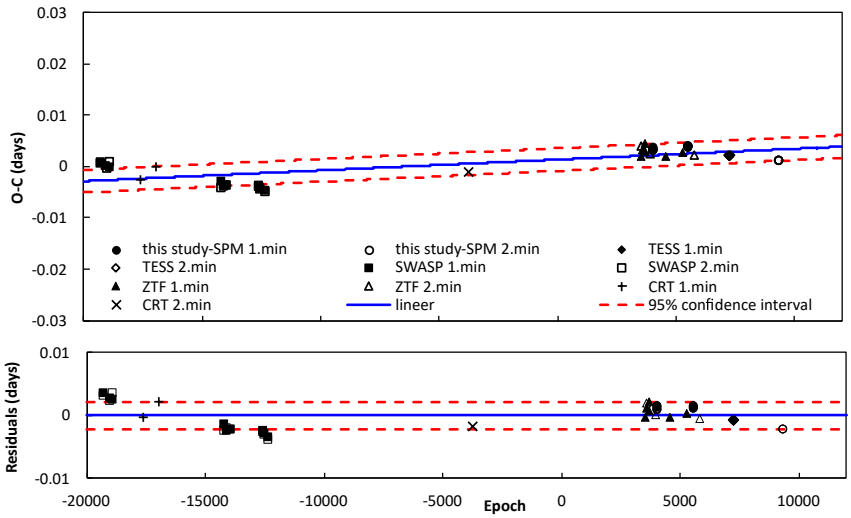

Fig. 1. According to all primary and secondary minimum times, the (O-C) diagram of the short period V840 Lyr binary. The blue solid line depicts a linear fit. In the lower panel, residuals pertaining to the linear ephemerides are shown. The red dashed lines represent a 95% confidence interval. The color figure can be viewed online.

Using equation 4, we found the revised period to be $0^{\rm d}.22131121$ for V840 Lyr.

The bottom panel of Figure 1 displays the residuals from equation 3, and Column 8 of Table 2 lists them.

4. THE SOLUTION OF THE PHOTOMETRIC LIGHT CURVE

In this work, the V, R_c and I_c light curves described above are used. The W-D code-based `Phoebe0.31a` interface program was used to analyze the light curves of V840 Lyr in order to understand its geometrical structure and evolutionary state (Wilson & Devinney 1971; Wilson 1979; van Hamme & Wilson 2003; Wilson et al. 2010; van Hamme 1993). The O'Connell effect can be seen in the binary system's light curves, and it can be explained by dark-cool spot activity on the secondary component (Qian et al. 2017). The O'Connell effect can be modeled by placing a spot on any of the system components. At the same time, the study of Kallrath & Milone (1999) explains how to determine the hotter and cooler spot. As specified by Kallrath & Milone (1999), '*colour amplitudes increase when going to $V \rightarrow R \rightarrow I$ as expected for cool spots*'. The opposite of this is valid for the hotter spot. In this study, the cooler spot was placed on the secondary component of the V840 Lyr system. Modeling can be done also by placing a cooler spot on the primary component. The best fit is obtained in the case with the cooler spot on the secondary component. We applied a second-order polynomial regression to the sample data of Berdyugina (2005) to determine the spot's temperature factor. A polynomial fit to the change in temperature ΔT between spot and photosphere temperatures is given by:

$$\begin{aligned}\Delta T &= (T_{phot} - T_{spot}) \\ &= 2.89 \times 10^{-5}\, T_{phot}^2 + 0.34\, T_{phot} - 1088\,,\end{aligned} \tag{5}$$

where T_{spot} and T_{phot} are spot and photosphere temperatures, respectively. For the cooler spots, the temperature factor is less than 1. Several groups of spots are tested. Finally, a converged solution was found with a cooler spot on the secondary components of V840 Lyr system. The solution parameters for the V840 Lyr system are listed in Table 4. The light curves in Figure 4 demonstrate common EW-type changes that make it possible to identify accurate photometric parameters. 2MASS provided magnitudes in the J, H and K bands (12.851, 12.299, and 12.219 mag, respectively) (Cutri et al. 2003). The spectral class of V840 Lyr is K3 or K5, according to the color indices $J - H = 0.552$ mag and $H - K = 0.632$ mag. The Planck function representing the black-body radiation is given by

$$B_\lambda(\lambda, T) = \frac{2hc^2}{\lambda^5} \frac{1}{\exp(\frac{hc}{\lambda kT}) - 1}\,, \tag{6}$$

where $B_\lambda, h, c, \lambda, k$, and T represent the spectral radiance, the Planck constant, the speed of light, the wavelength, the Boltzman constant, and the temperature, respectively. This function was fitted to the Gaia energy distribution spectrum of the V840 Lyr binary star system. The temperature that provided the best fit was 4820 K (see Figure 2). The light curve solutions were carried out by keeping this temperature value (4820 K) constant.

TABLE 2

NEW CCD MINIMUM TIMES FOR V840 LYR, FROM SPM AND OTHER SURVEYS

Observed BJDmin(2.4M+)	Instrument (filter)	Min I/II	Ref.	Observed BJDmin(2.4M+)	Instrument (filter)	Min I/II	Ref.
53143.68187	CCD	Min.II	(1)	58305.76370	I_c	Min.II	(4)
53144.67801	CCD	Min.I	(1)	58305.87452	R_c	Min.I	(4)
53201.55432	CCD	Min.I	(1)	58305.87460	I_c	Min.I	(4)
53204.54147	CCD	Min.II	(1)	58305.87476	V	Min.I	(4)
53231.54280	CCD	Min.II	(1)	58305.98481	V	Min.II	(4)
53232.53755	CCD	Min.I	(1)	58305.98539	R_c	Min.II	(4)
53526.87864	CCD	Min.I	(2)	58427.59401	CCD	Min.I	(3)
53669.62683	CCD	Min.I	(2)	58588.93059	CCD	Min.I	(3)
54275.57350	CCD	Min.I	(1)	58640.93952	I_c	Min.I	(4)
54276.56826	CCD	Min.II	(1)	58640.93956	R_c	Min.I	(4)
54297.59319	CCD	Min.II	(1)	58640.93980	V	Min.I	(4)
54298.58886	CCD	Min.I	(1)	58641.93571	I_c	Min.II	(4)
54327.47016	CCD	Min.II	(1)	58641.93576	V	Min.II	(4)
54328.46606	CCD	Min.I	(1)	58641.93584	R_c	Min.II	(4)
54628.56379	CCD	Min.I	(1)	58700.80260	CCD	Min.II	(3)
54628.67418	CCD	Min.II	(1)	59012.18724	CCD	Min.II	(5)
54644.49783	CCD	Min.I	(1)	59012.51913	CCD	Min.I	(5)
54645.49342	CCD	Min.II	(1)	59019.82226	CCD	Min.I	(5)
54683.44789	CCD	Min.I	(1)	59019.93293	CCD	Min.II	(5)
54684.44347	CCD	Min.II	(1)	59023.36325	CCD	Min.I	(5)
56592.59073	CCD	Min.II	(2)	59023.47392	CCD	Min.II	(5)
58204.95510	CCD	Min.I	(3)	59024.35929	CCD	Min.II	(5)
58205.95317	CCD	Min.II	(3)	59024.46998	CCD	Min.I	(5)
58210.93182	CCD	Min.I	(3)	59034.53962	CCD	Min.II	(5)
58235.93964	CCD	Min.I	(3)	59034.87159	CCD	Min.I	(5)
58237.93292	CCD	Min.I	(3)	59484.68517	I_c	Min.II	(4)
58290.93488	CCD	Min.II	(3)	59484.68518	R_c	Min.II	(4)
58305.76346	V	Min.II	(4)	59484.68519	V	Min.II	(4)
58305.76355	R_c	Min.II	(4)				

Equation 2 is used to calculate the minima, with Min.I denoting the primary minimum and Min.II denoting the secondary minimum. Ref: (1) SWASP, (2) CRTS, (3) ZTF, (4) SPM-This study, (5) TESS-This study.

This temperature value (4820 K) is among the temperature values found from other surveys and catalogues in Table 3. Therefore, T_1 = 4820 K was chosen as the major component's effective temperature, and we kept this temperature value constant during the solution process and analysis. Estimated values for the relevant effective temperatures obtained from the other surveys and catalogues are between 4910 K and 4535 K. A list showing these temperature values is given in Table 3.

The depths of both minima in the light curves are approximately equal, indicating that both components are roughly at the same temperature. The gravity-darkening coefficients and bolometric albedo are therefore set to the same values for both components, $g_1 = g_2 = 0.32$ (Lucy 1967) and $A_1 = A_2 = 0.5$ (Ruciński 1969). According to Claret & Gimenez (1990), the bolometric and bandpass limb-darkening coefficients (x and y) were applied to model the light curves. The parameters include the star 1 and star 2's dimensionless potential ($\Omega_1 = \Omega_2$ for mode 3-overcontact configuration), star 1's orbital inclination (i), star 2's mean temperature (T_2), and the star 1's monochromatic luminosities ($L_{1,V}$, L_{1,R_c}, L_{1,I_c}).

The mass ratio of the system was determined using the q-search technique ($q = M_2/M_1$). For a variety of mass ratio values, solutions were obtained. We discovered that the answers typically converged to mode 3 for each value of q. The calculation began in mode 2 (detached mode) for each value of q. Figure 3 shows

TABLE 3

EFFECTIVE TEMPERATURE AND SPECTRAL CLASSIFICATIONS FOR V840 LYR ACCORDING TO SEVERAL CATALOGUES

Catalogue / Survey	$(J–H)_0$	$\pm\sigma$	T^a_{eff}	BC^b	Spt.Type^c
2MASS (Cutri et al. 2003)	0.537	0.115	4535*	-0.61*	K4.5*
TESS Input Catalog (Paegert et al. 2021)	0.455	0.122	4910*	-0.37*	K2.6*
APASS DR9 (Henden et al. 2015)	0.505	0.085	4718*	-0.49*	K3.6*
Worthey & Lee (2011)	0.540	0.101	4758	-0.41	K3.4*
Gaia DR2 (Gaia Collaboration et al. 2018)	0.485	0.075	4801	-0.43*	K3.2*
Drilling & Landolt (2000)	0.537	0.135	4718	-0.50	K3.3

$E(J-H) = 0.015$ mag, a : T_{eff} of the primary component, b : bolometric correction, c : spectral class of the primary component, $*$: estimated by Pecaut & Mamajek (2013).

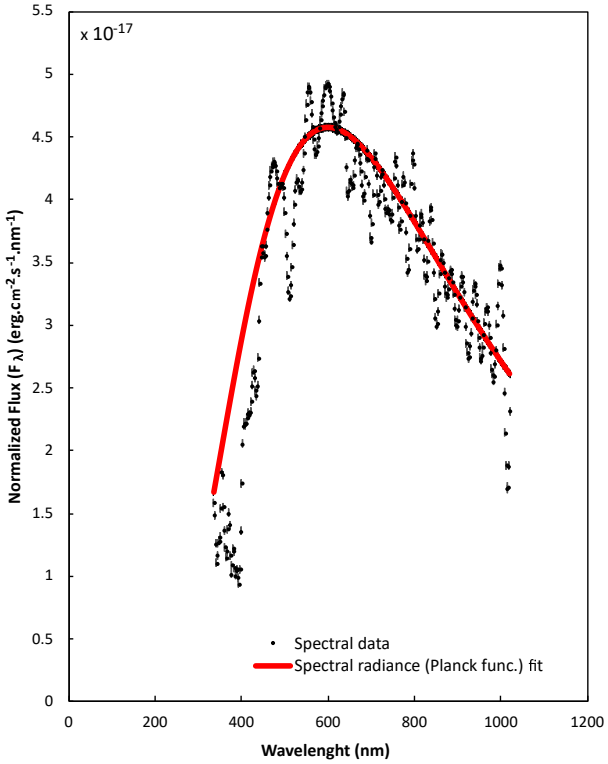

Fig. 2. The Gaia energy distribution spectrum of the V840 Lyr binary star system. The black dots along with the errors show the spectral data of the system. The red solid line depicts a black-body (Planck function) fit. The color figure can be viewed online.

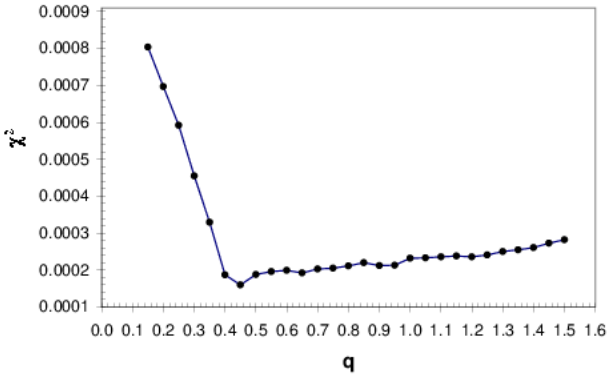

Fig. 3. The relation between χ^2 and q for V840 Lyr, and the minimum is found at $q = 0.45$. The color figure can be viewed online.

the relationship between q and the sum of the results of the weighted squared deviations, χ^2. A minimum is discovered at $q = 0.45$, as represented in the figure. At $q = 0.45$, the value of χ^2 is 0.00016. As a result, we decided to make q an adjustable parameter and set its initial value at 0.45. Models were solved by considering together the light curves of SPM observations in the V, R_c and I_c bands and TESS observations. During the light curve-LC analysis processes of SPM and TESS, we kept the primary temperature T_1, the initial epoch T_0, the period of the system P, and semi-major axis $(SMA) - a(\mathrm{R}_\odot)$ parameters constant and left free the mass ratio q, the inclination of the system i, the secondary temperature T_2, the potential of the components $\Omega_1 = \Omega_2$. The q value changed little from the initial value determined by the $q - search$ process during the analysis process. In the analysis processes, the third light contribution was also investigated. Observational errors are in the range of 0.01 to 0.02 by taking into account weights on data in the standard $1/\sigma^2$ form. The light curve analysis was performed by taking into account the observation weights. The propagation errors of the solution parameters were determined using the well-known astrophysical equations. These errors are given in Table 4 and Table 5.

Final solutions were derived after applying differential corrections until they converged. For no third light and third light, our solution respectively converged at $q = 0.4509 \pm 0.0705$ and $q = 0.4543 \pm 0.0710$. The synthetic/model light curves estimated using those photo-

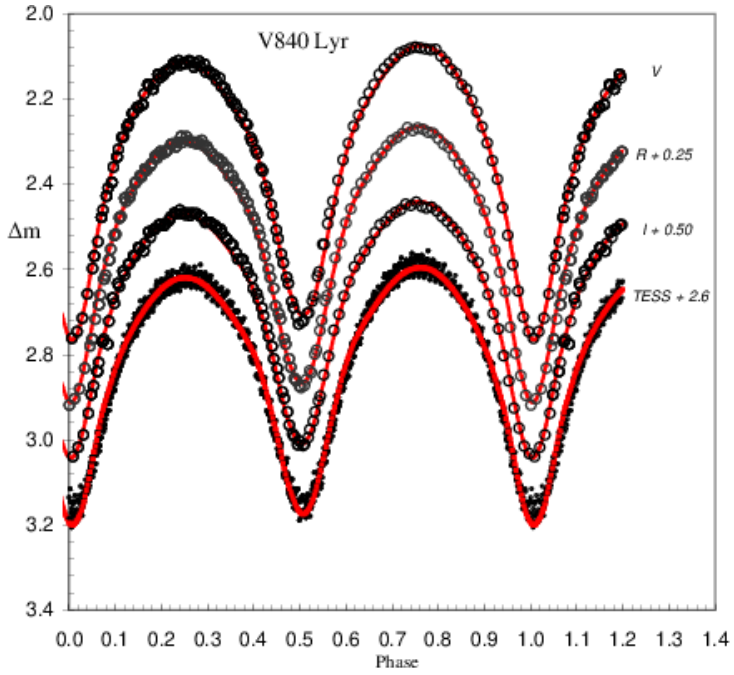

Fig. 4. The photometric light curves and synthetic/model fit with the dark-colder spot (solid-red line) of V840 Lyr in the V, R_c and I_c filters. The observational light curve and synthetic/model fit of TESS data are given at the bottom. The color figure can be viewed online.

metric solution parameters which are given in Columns 3 and 5 of Table 4, are presented in Figure 4. Because of how asymmetric the light curves are, the spotted solution is required. The solution reveals that V840 Lyr is a W-subtype W UMa contact binary with a mass ratio of $q = 0.4509 \pm 0.0705$ and a degree of contact factor of $f = 15.14\% \pm 5.68\%$. Figures 5 and 6 display the Roche geometrical structures of the system at different phases as well as the outline of the Roche surface.

5. ABSOLUTE PARAMETERS

For V840 Lyr a W-subtype W UMa binary system, we estimated the absolute parameters listed in Table 5 using the best model for the 2020 light curves as a guide. Without radial velocity information, the total mass cannot be calculated directly. The binary stars' masses, radii, and luminosities are, however, listed from the literature.

The absolute parameters were calculated using statistical relationships. For short period binaries with $P < 0^{\rm d}.27$, which include radial velocity and contemporary light curve solutions, Dimitrov & Kjurkchieva (2015) discovered an empirical relation that is well defined between the a-semi major axis and P-period. Because we lacked information on radial velocity, we used their relationship to estimate the a-semi major axis of the system orbit, which is given by

$$a(\mathrm{R}_\odot) = -1.154 + 14.633 \times P - 10.319 \times P^2, \quad (7)$$

with the parabolic fit's standard error given as $0.05\mathrm{R}_\odot$. The semi major axis of the target system V840 Lyr is estimated to be $a(\mathrm{R}_\odot) = 1.57903 \pm 0.08059$ using its orbital period. During the photometric solution using `Phoebe0.31a`, this value is fixed. Equation 7 was used to obtain the error in a from the error in P and is responsible for the error value of 0.08059 stated for the semi-major axis.

The V840 Lyr eclipsing binary system's q mass ratio was estimated to be 0.4509 ± 0.0705. We calculated the primary star's mass for the V840 Lyr eclipsing binary system using the $a(\mathrm{R}_\odot)$-semi major axis values, the q-mass ratio, $q = M_2/M_1$, and the corrected third law of Kepler, $M_1(1 + q) = a^3/P^2$. Thus it was calculated to be $M_1 = 0.744 \pm 0.097\mathrm{M}_\odot$. Then, using the fractional radii ($r_{1,2}$) and the semimajor axis values-$a(\mathrm{R}_\odot)$, we calculated the radii of the target system's component stars in units of solar radii using the formula $r_{1,2} = R_{1,2}/a$. Table 5 shows the outcomes of our calculations using equation 7 for the absolute parameters. In addition, the final information about the system obtained from GaiaDR3 (Gaia Collaboration 2022) and TESS (Stassun et al. 2019) observation results is given in Table 5. Also, the additional photometric elements-based absolute parameters for the *V840Lyr* system were $M_2 = 0.336 \pm 0.052\mathrm{M}_\odot$, $R_1 = 0.735 \pm 0.039\mathrm{R}_\odot$, and $R_2 = 0.508 \pm 0.029\mathrm{R}_\odot$.

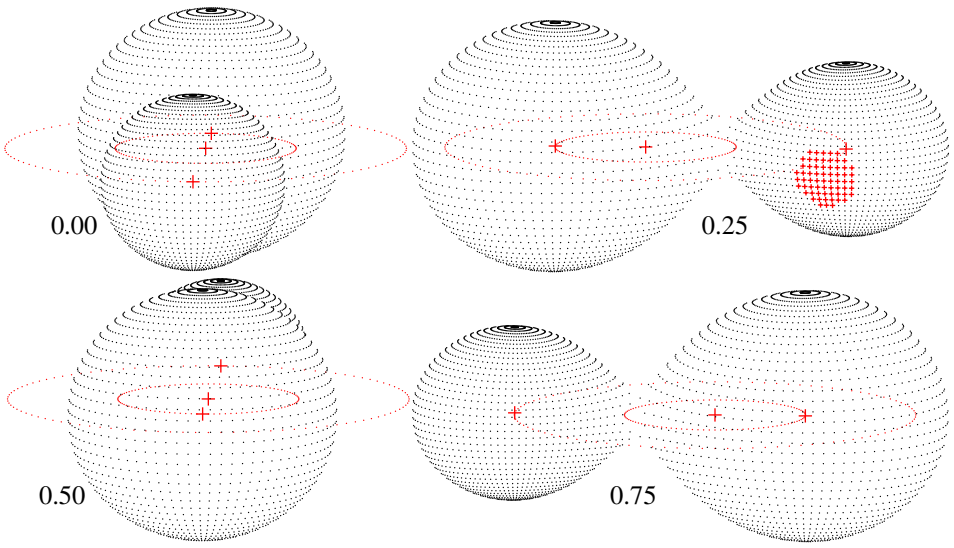

Fig. 5. The W-type contact binary V840 Lyr's Roche configuration at phases 0.00, 0.25, 0.50, and 0.75. The color figure can be viewed online.

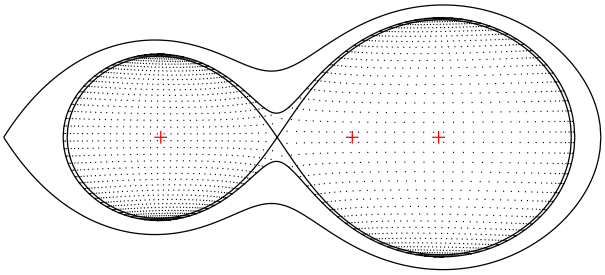

Fig. 6. The V840 Lyr binary system Roche surface outline pattern. The color figure can be viewed online.

Lucy & Wilson (1979) calculated the fill-out parameter (f), which indicates the degree of contact between companion stars in a binary system using the formula $f = (\Omega_{inner} - \Omega)/(\Omega_{inner} - \Omega_{outer})$. Here, Ω_{outer} stands for the outer critical Lagrangian/Roche equipotential, Ω_{inner} is the critical Lagrangian equipotential of the inner critical Roche surface, and $\Omega = \Omega_{1,2}$ indicates the surface Lagrangian/Roche equipotential of the component stars and varies from 0 (the inner critical Roche surface) to 1 (the outer critical Roche surface). Since the computed fill-out parameter of V840 Lyr was $f = 0.1514$, we came to the conclusion that the target system is a contact binary.

Using the astrophysical well-known equations:

$$\frac{L_\star}{L_\odot} = 10^{-0.4(M_{bol,\star} - M_{bol,\odot})}\ ,$$
$$M_{bol,sys} = M_{bol,\star} + 2.5 \log \frac{L_\star}{L_{sys}}\ , \quad (8)$$

where the prefix ($\star$) refers to system component stars, and $M_{bol,\odot} = 4.74$ mag (Cox 2000). $M_{bol,system} = 5^m.83$ is the system's bolometric absolute magnitude, we calculated the system's bolometric absolute magnitude from the individual bolometric absolute magnitudes ($M_{bol,1} = 6^m.26$, $M_{bol,2} = 7^m.05$) of the components obtained from the `Phoebe` solution and also the luminosities of the component stars.

The $\log(g)$ values of V840 Lyr are compatible with the values calculated to be $\log(g_1) = 4.58 \pm 0.10$ cgs, $\log(g_2) = 4.55 \pm 0.11$ cgs using the primary and secondary component's masses and radii within an error range. The equations of Mochnacki (1981) were used to get the components' mean densities of the V840 Lyr binary system and the components' mean densities were computed to be $\rho_1 = 2.80 \pm 0.14$ gr cm^{-3} and $\rho_2 = 3.67 \pm 0.20$ gr cm^{-3}.

We used the IPAC's database given in NASA/Extragalactic and the reddening maps from Schlafly & Finkbeiner (2011) for the interstellar extinction value (A_v) to the distance of the V840 Lyr binary system,

$$d(\mathrm{pc}) = 10^{(m - M_v - A_v + 5)/5}\ , \quad (9)$$

to be 443.6 ± 28.2 pc using $M_{bol}(system) = 5.83$ mag and $BC = -0.02$ mag, assuming that they are main sequence stars and considering $A_v = 0.1918$ for the interstellar extinction. The Gaia EDR3 catalogue lists V840 Lyr's parallax as 2.2298 ± 0.0214 mas. The system's Gaia distance is 448.5 ± 5.3 pc. This value is consistent with our distance estimation.

TABLE 4

V840 LYR'S SOLUTION PARAMETERS WITH DARK, COOLER SPOT

		No third light		Third light	
Description	Parameters	Values	$\pm\sigma$	Values	$\pm\sigma$
The initial point of the ephemeris	T_0 (HJD)	2457422.6180	fixed	2457422.618	fixed
Orbital period	P (days)	0.221311	fixed	0.221311	fixed
Semi major axis	*SMA* ($R_\odot$)	1.57903	fixed	1.57903	fixed
Mass ratio	q	0.4509	0.0705	0.4543	0.0710
Orbital inclination	i	80.44	0.09	80.49	0.07
Fill-out parameter	f	0.1514	0.0568	0.2323	0.0871
The ratio of frac. radii	$k = r_2/r_1$	0.6919		0.6986	
Temperature ratio	T_2/T_1	0.9907		0.9913	
Temperature of primary comp.	T_1 (K)	4820	fixed	4820	fixed
Temperature of secondary comp.	T_2 (K)	4775	110	4778	112
Surface potential of components	$\Omega_1 = \Omega_2$	2.7389	0.0052	2.7234	0.0044
Bol. albedo of components	$A_1 = A_2$	0.50		0.50	
Gravity darkening exponents	$g_1 = g_2$	0.32		0.32	
Bolometric limb darkening	(V)	0.800, 0.066		0.800, 0.066	
Logarithmic coefficients of	(R_c)	0.721, 0.146		0.721, 0.146	
pri. component (x_1 , y_1)	(I_c)	0.625, 0.175		0.625, 0.175	
Bolometric limb darkening	(V)	0.800, 0.066		0.800, 0.066	
Logarithmic coefficients of	(R_c)	0.721, 0.146		0.721, 0.146	
sec. component (x_2 , y_2)	(I_c)	0.625, 0.175		0.625, 0.175	
The fractional luminosities	(V)	0.6816	0.0251	0.6778	0.0820
of primary component	(R_c)	0.6802	0.0260	0.6736	0.0891
$L_1/(L_1 + L_2)$	(I_c)	0.6794	0.0272	0.6656	0.0942
The fractional luminosities	(V)	0.3184	0.0252	0.3222	0.0822
of secondary component	(R_c)	0.3198	0.0263	0.3264	0.0890
$L_2/(L_1 + L_2)$	(I_c)	0.3205	0.0271	0.3344	0.0941
Third light	l_3 (V)	0		0.0020	0.0007
	l_3 (R_c)	0		0.0011	0.0008
	l_3 (I_c)	0		0.0033	0.0009
The frac. radii of	$r_1(pole)$	0.4351	0.0012	0.4302	0.0010
primary component	$r_1(side)$	0.4658	0.0014	0.4595	0.0011
	$r_1(back)$	0.4969	0.0039	0.4899	0.0033
The frac. radii of	$r_2(pole)$	0.2994	0.0014	0.2993	0.0011
secondary component	$r_2(side)$	0.3138	0.0017	0.3133	0.0013
	$r_2(back)$	0.3539	0.0031	0.3513	0.0023
The mean frac. radii of pri. comp.	$r_{1,mean}$	0.4659	0.0018	0.4598	0.0015
The mean frac. radii of sec. comp.	$r_{2,mean}$	0.3224	0.0020	0.3213	0.0016
Spot parameters of the secondary component					
Spot co–latitude	Θ [°]	100.00	3.82	100.00	3.82
Spot longitude	ϕ [°]	80.00	1.93	80.00	1.93
Angular radius	r_s [°]	20.00	1.75	20.00	1.75
Temperature factor	fraction	0.7376		0.7376	

Note: The errors ($\pm\sigma$) are solely formal errors generated by `Phoebe0.31a`. They are the modeling-related propagating uncertainties.

TABLE 5

THE ABSOLUTE PARAMETERS OF V840 LYR

Description	**Parameters**	**This Study values $\pm\sigma$**	**Gaia-DR3[a] values $\pm\sigma$**	**Tess[b] values $\pm\sigma$**
The first Lagrangian point's equipotential	$\Omega(L_1)$	2.773046		
The second Lagrangian point's equipotential	$\Omega(L_2)$	2.502974		
The primary comp.'s mass	$M_1(\mathrm{M}_\odot)$	0.744 ± 0.097	0.754 ± 0.043	0.760
The secondary comp.'s mass	$M_2(\mathrm{M}_\odot)$	0.336 ± 0.052	0.341 ± 0.019	0.343
The primary comp.'s radius	$R_1(\mathrm{R}_\odot)$	0.735 ± 0.039	0.757 ± 0.018	0.774
The secondary comp.'s radius	$R_2(\mathrm{R}_\odot)$	0.508 ± 0.029	0.523 ± 0.013	0.535
The primary comp.'s temperature	$T_1(\mathrm{K})$	4820	4829 ± 33	4726 ± 155
The secondary comp.'s temperature	$T_2(\mathrm{K})$	4775 ± 110	4784 ± 33	4682 ± 155
The primary comp.'s bol. absolute magnitude	$M_1^{bol}(\mathrm{mag})$	6.26 ± 0.12		
The secondary comp.'s bol. absolute magnitude	$M_2^{bol}(\mathrm{mag})$	7.05 ± 0.13		
The primary comp.'s logarithmic surface gravity	$\log(g_1)(\mathrm{cgs})$	4.58 ± 0.10	4.56 ± 0.02	4.54
The secondary comp.'s logarithmic surface gravity	$\log(g_2)(\mathrm{cgs})$	4.55 ± 0.11	4.53 ± 0.02	4.51
The primary comp.'s luminosity	$L_1(\mathrm{L}_\odot)$	0.257 ± 0.052	0.257 ± 0.007	0.269
The secondary comp.'s luminosity	$L_2(\mathrm{L}_\odot)$	0.119 ± 0.025	0.119 ± 0.003	0.125
The primary comp.'s density	ρ_1 (gr cm^{-3})	2.80 ± 0.14	2.45 ± 0.01	2.31
The secondary comp.'s density	ρ_2 (gr cm^{-3})	3.67 ± 0.20	3.35 ± 0.01	3.03
Distance of the system	d(pc)	443.6 ± 28.2	448.5 ± 5.3	444.0 ± 4.2
Total mass	$M_t(\mathrm{M}_\odot)$	1.080 ± 0.149	1.094 ± 0.062	1.103
The system's mass function	$f(M_t)(\mathrm{M}_\odot)$	1.036 ± 0.151	1.049 ± 0.068	1.057

a; Ref; Gaia Collaboration (2022), b; Ref; Stassun et al. (2019).

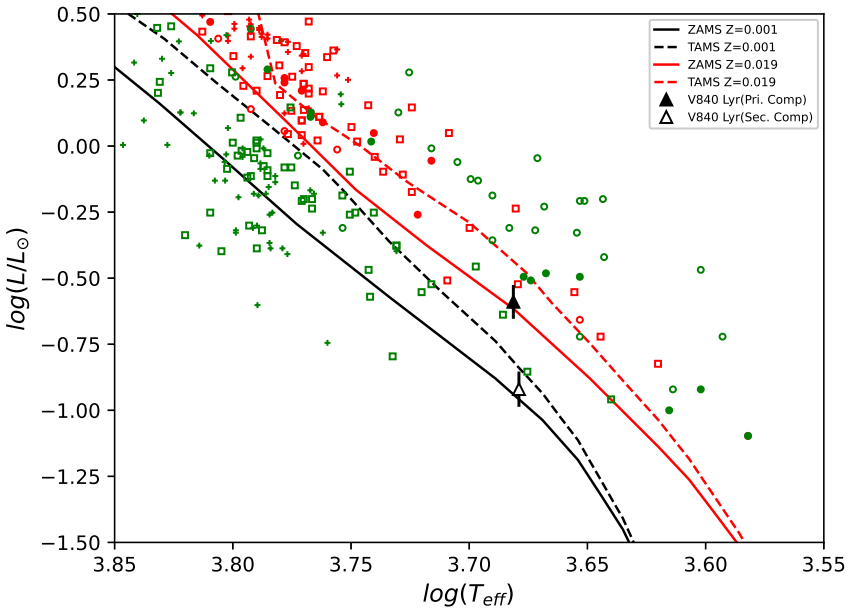

Fig. 7. The locations of V840 Lyr along the ZAMS and TAMS lines from Girardi et al. (2000) (Z = 0.001 and 0.0019) on the HR diagram. The black-filled and empty triangles display V840 Lyr's primary and secondary stars. The example systems of Yakut & Eggleton (2005) are presented. '□'; W-type, '+'; A-type example contact W UMa binaries, '○'; example binaries close to contact, and '●'; detached example binaries. Red colors represent every primary star, green colors every secondary star. Temperature errors stay within the symbol size. The color figure can be viewed online.

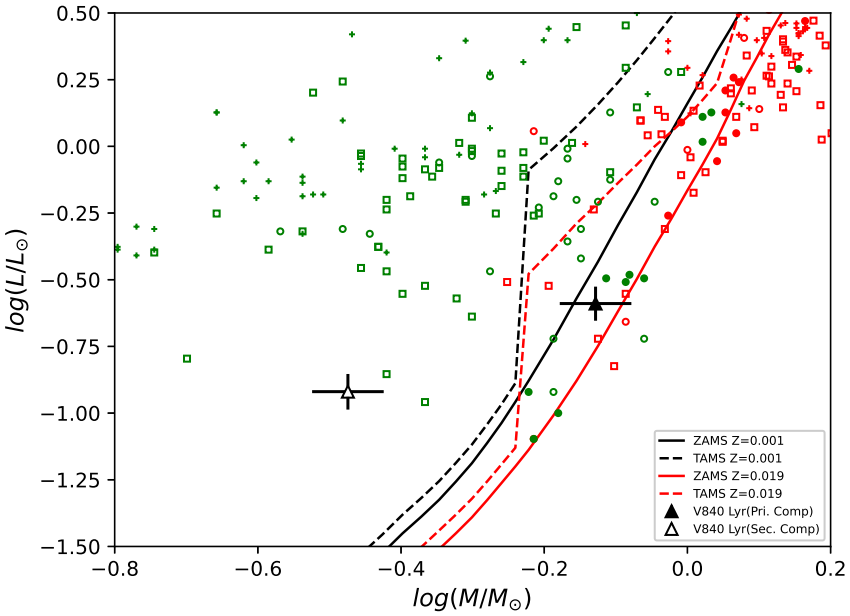

Fig. 8. V840 Lyr's location on the mass-luminosity diagram. The sample systems, symbols, and other details are indicated in Figure 7. The color figure can be viewed online.

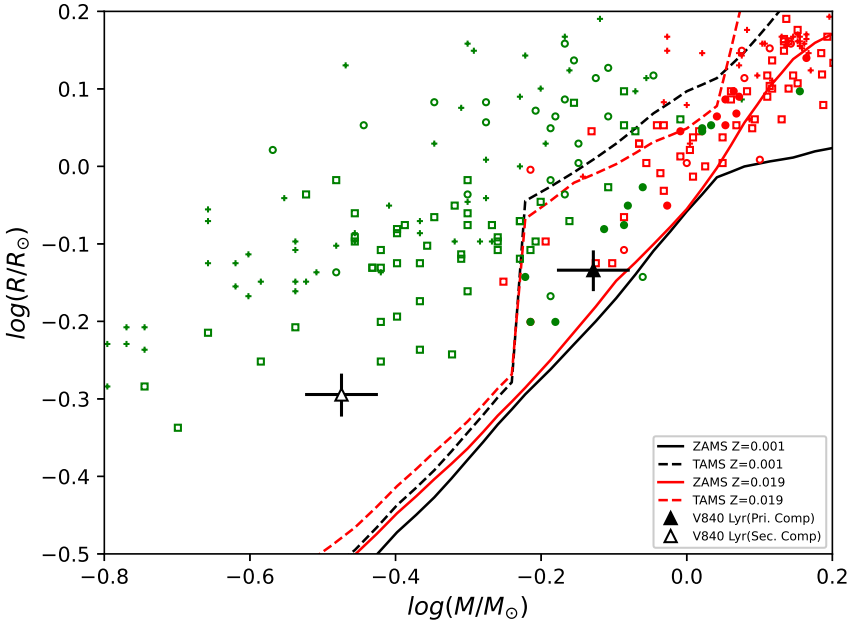

Fig. 9. V840 Lyr location on the mass-radius diagram. The sample systems, symbols, and other details are indicated in Figure 7. The color figure can be viewed online.

We display on the HR $(Hertzsprung\ Russell)$, $M\ (mass) - L\ (luminosity)$, $M\ (mass) - R\ (radius)$, $M\ (mass) - J_0\ (momentum)$ diagrams and also on the HR diagram with the evolutionary tracks, the position of V840 Lyr together with the other contact binaries in Figures 7-11, respectively.

6. DISCUSSION AND CONCLUSIONS

The asymmetrical light curves of V840 Lyr we acquired from the SPM observatory show the O'Connell effect. It is clear that the maximum level at phase 0.75 of our multicolour light curves is, respectively, around 0.033 mag, 0.030 mag, and 0.024 mag higher than those

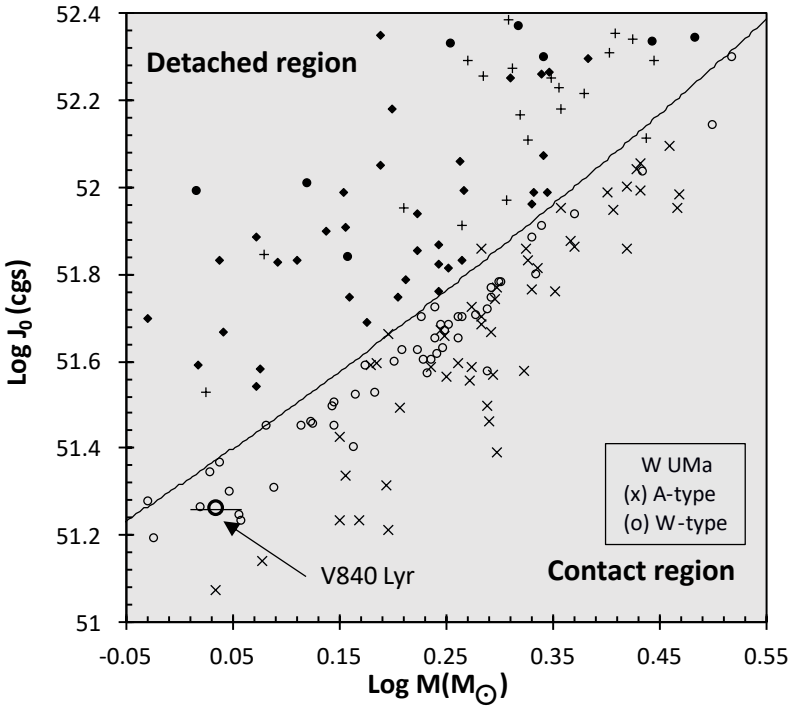

Fig. 10. The location of V840 Lyr on the mass-angular momentum diagram according to Eker et al. (2006), under the J_{lim} borderline dividing detached and contact binaries. The symbols are the same ones that are described in Figures 1 and 4 of Eker et al. (2006)'s study. The circles show the W-subtype systems, whereas the crosses stand for the A-subtype systems. The error of $\log J_0$ is within the size of the symbol. The color figure can be viewed online.

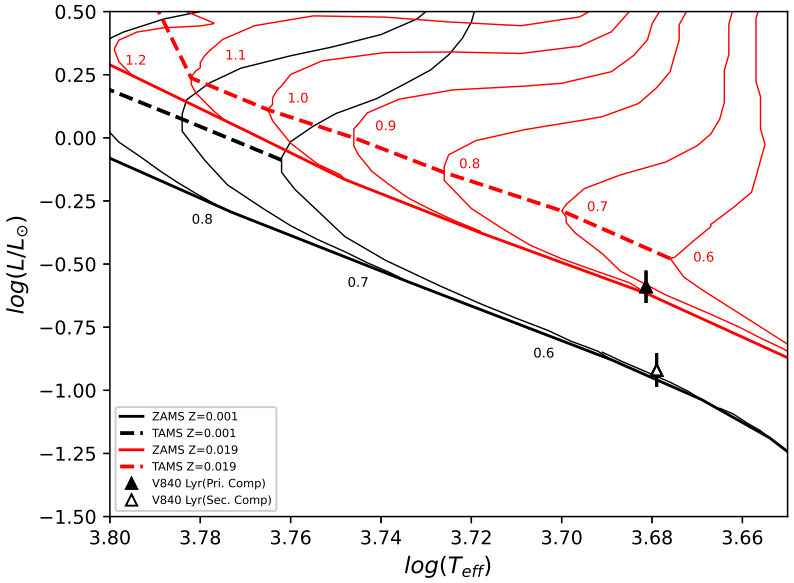

Fig. 11. V840 Lyr's components (triangles) plotted in the HR diagram with ZAMS, TAMS, evolutionary tracks and isochrone derived from Girardi et al. (2000) for Z = 0.001 and 0.019. The errors are within the symbol's size. The color figure can be viewed online.

at phase 0.25 despite the fact that the Min-I and Min-II minimum depths of our multicolour light curves are nearly equal. The light curves we acquired do not demonstrate a large scatter, as shown in Figure 4. This suggests that more credible solutions might be found using our light curves.

The secondary component's dark-cool spot was considered to account for the asymmetries in our light curves. With the help of the `Phoebe0.31a` interface software based on the WD method, we discovered that V840 Lyr is an extreme mass ratio ($q = 0.4509$) W-subtype contact W UMa type binary star with a 15.14% fill-out factor. The photometric results showed that the more massive component's temperature is about 45 K higher than that of the less massive component. Over four years, V840 Lyr was observed, and 17 times of light minima were discovered.

According to the absolute parameters estimated in this work, the angular momentum $\log J_0$ value of V840 Lyr is 51.261 in cgs units, and the $\log J_{lim} = 51.371$ in cgs units using the angular momentum expression of Eker et al. (2006). These values of $\log J_0$ are less than those of $\log J_{lim}$ ($\log J_0 < \log J_{lim}$). This result shows that V840 Lyr, according to the absolute parameter estimations, is located in the contact configuration region of the angular momentum diagram obtained by Eker et al. (2006) (see Figure 10).

We compared the component locations of the target system with LTCBs (A type), LTCBs (W type), NCBs, and DCBs samples in the $M - L$, $M - R$, $M - J_0$, and $T_{eff} - L$ diagrams with ZAMS and TAMS provided by Girardi et al. (2000), taking into account the absolute parameters we obtained for the V840 Lyr binary system (see Figures 7-11). V840 Lyr resembles other contact binary systems (Yakut & Eggleton 2005; Eker et al. 2006). Using evolutionary tracks and isochrones, we also determine the evolutionary status of the V840 Lyr binary system.

Regarding the absolute parameters of the primary component, V840 Lyr is also compatible with the evolutionary tracks for $0.74\,\mathrm{M}_{\odot}$, a single star with metallicities of Z=0.019 and Z=0.001. It is possible to determine that the V840 Lyr's primary and secondary components positions in the HR diagram, compared with stellar evolutionary paths, are appropriate for the binary system masses. The primary and secondary stars of the V840 Lyr were positioned on the ZAMS with a Z=0.019 and Z=0.001 metallicity, respectively, as shown in Figures 7 and 9. It is plausible that the system's constituents were exchanging mass with one another; from the secondary to the primary star (see Figure 1).

Using the Binary Maker 3.0 tool (Bradstreet & Steelman 2002), we created Roche configurations of the components that make up the V840 Lyr in accordance with the target system's absolute parameters (see Figure 5-6).

Using the estimated absolute parameters, we computed the distance of the V840 Lyr to be $d = 443.6 \pm 28.2$ pc, consistent with the distance ($d = 448.5 \pm 5.3$ pc) obtained from the Gaia EDR3's parallax (2.2298 ± 0.0214 mas) (see Table 5). Additionally, the absolute parameters obtained in this study were compared with GaiaDR3 (Gaia Collaboration 2022) and TESS (Stassun et al. 2019) data and are given in Table 5. As a result of this comparison, it can be seen that the absolute parameters obtained from the analysis are consistent with the results of GaiaDR3 and TESS.

In summary, V840 Lyr is quite remarkable and seems to be an overcontact binary star. The stars that make up our target binary system have filled Roche lobes. The target system V840 Lyr's estimated absolute parameters are roughly within the predicted limits, as demonstrated by a comparison with the other W UMa stars. However, the absolute solution parameters of the target system V840 Lyr in this work should be considered as preliminary values in the absence of spectroscopic studies, which are necessary for the more reliable identification of the spectral types, the semi-major axis, and the mass ratio.

Combining more sensitive photometric and spectroscopic observations of this binary star would be a significant step forward in advancing our comprehension of contact binaries, validating the existing results, and revealing the true structure of this system. We encourage researchers to do the appropriate photometric and spectroscopic measurements to confirm the existence of starspots and establish their locations. This will help us to learn more about this system.

We thank the San Pedro Martir National Astronomical Observatory (SPM) for its support in allowing us the use of its T84 telescope, and Edilberto Sánchez-Moreno (IAUNAM) for help with some of our figures. We gratefully acknowledge the SIMBAD, ADS, CRTS, TESS, BRNO O-C Gateway, Kraków O-C Atlas, NASA/IPAC, and Gaia EDR3 databases for also providing data. We acknowledge with thanks the variable star observations from the AAVSO International Database contributed by observers worldwide and used in this research. This publication makes use of data products from the Two Micron All Sky Survey, which is a joint project of the University of Massachusetts and the Infrared Processing and Analysis Center/California Institute of Technology, funded by the National Aeronautics and Space Administration and the National Science Foundation. We also thank the anonymous referee for her/his valuable comments to improve this article.

REFERENCES

Bellm, E. C., Kulkarni, S. R., Graham, M. J., et al. 2019, PASP, 131, 018002, https://doi.org/10.1088/1538-3873/aaecbe

Berdyugina, S. V. 2005, LRSP, 2, 8, https://doi.org/10.12942/lrsp-2005-8

Bradstreet, D. H. & Steelman, D. P. 2002, AAS, 34, 1224
Claret, A. & Gimenez, A. 1990, A&A, 230, 412
Cox, A. N. 2000, Allen's astrophysical quantities, 4th ed. (New York, NY: AIP)
Cutri, R. M., Skrutskie, M. F., van Dyk, S., et al. 2003, VizieR Online Data Catalog, II/246
Dimitrov, D. P. & Kjurkchieva, D. P. 2015, MNRAS, 448, 2890, https://doi.org/10.1093/mnras/stv147
Drake, A. J., Djorgovski, S. G., Mahabal, A., et al. ApJ, 696, 870, https://doi.org/10.1088/0004-637X/696/1/870
Drilling, J. S. & Landolt, A. U. 2000, in Allen's Astrophysical Quantities, ed. A. N. Cox, 381
Eastman, J., Siverd, R., & Gaudi, B. S. 2010, PASP, 122, 935, https://doi.org/10.1086/655938
Eker, Z., Demircan, O., Bilir, S., & Karataş, Y. 2006, MNRAS, 373, 1483, https://doi.org/10.1111/j.1365-2966.2006.11073.x
Gaia Collaboration. 2022, VizieR Online Data Catalog, I/355
Gaia Collaboration;, Brown, A. G. A., Vallenari, A., et al. 2018, A&A, 616, 1, https://doi.org/10.1051/0004-6361/201833051
Girardi, L., Bressan, A., Bertelli, G., & Chiosi, C. 2000, A&AS, 141, 371, https://doi.org/10.1051/aas:2000126
Henden, A. A., Levine, S., Terrell, D., & Welch, D. L. 2015, AAS, 225, 336.16
Hut, P. 1980, A&A, 92, 167
Kallrath, J. & Milone, E. F. 1999, in Eclipsing binary stars: modeling and analysis (New York, NY: Springer-Verlag), https://doi.org/10.1007/978-1-4419-0699-1
Lucy, L. B. 1967, ZA, 65, 89
Lucy, L. B. & Wilson, R. E. 1979, ApJ, 231, 502, https://doi.org/10.1086/157212
Mochnacki, S. W. 1981, ApJ, 245, 650, https://doi.org/10.1086/158841
Norton, A. J., Payne, S. G., Evans, T., et al. 2011, A&A, 528, 90, https://doi.org/10.1051/0004-6361/201116448
O'Connell, D. J. K. 1951, PRCO, 2, 85
Paegert, M., Stassun, K. G., Collins, K. A., et al. 2021, arXiv:2108.04778, https://doi.org/10.48550/arXiv2108.04778
Pecaut, M. J. & Mamajek, E. E. 2013, ApJS, 208, 9, https://doi.org/10.1088/0067-0049/208/1/9
Pollacco, D., Skillen, I., Collier Cameron, A., et al. 2006, Ap&SS, 304, 253, https://doi.org/10.1007/s10509-006-9124-x
Qian, S.-B., Han, Z.-T., Zhang, B., et al. 2017, ApJ, 848, 131, https://doi.org/10.3847/1538-4357/aa8bb8
Ruciński, S. M. 1969, AcA, 19, 245
Samus', N. N., Kazarovets, E. V., Durlevich, O. V., Kireeva, N. N., & Pastukhova, E. N. 2017, ARep, 61, 80, https://doi.org/10.1134/S1063772917010085
Schlafly, E. F. & Finkbeiner, D. P. 2011, ApJ, 737, 103, https://doi.org/10.1088/0004-637X/737/2/103
Stassun, K. G., Oelkers, R. J., Paegert, M., et al. 2019, AJ, 158, 138, https://doi.org/10.3847/1538-3881/ab3467
Sullivan, P. W., Winn, J. N., Berta-Thompson, Z. K., et al. 2015, ApJ, 809, 77, https://doi.org/10.1088/0004-637X/809/1/77
TESS. 2021, Observations from the Transiting Exoplanet Survey Satellite (TESS) International Database, https://archive.stsci.edu/missions-and-data/tess
van Hamme, W. 1993, AJ, 106, 2096, https://doi.org/10.1086/116788
van Hamme, W. & Wilson, R. E. 2003, ASPC, 298, 323
Wilson, R. E. 1979, ApJ, 234, 1054, https://doi.org/10.1086/157588
Wilson, R. E. & Devinney, E. J. 1971, ApJ, 166, 605, https://doi.org/10.1086/150986
Wilson, R. E., van Hamme, W., & Terrell, D. 2010, ApJ, 723, 1469, https://doi.org/10.1088/0004-637X/723/2/1469
Worthey, G. & Lee, H.-C. 2011, ApJS, 193, 1, https://doi.org/10.1088/0067-0049/193/1/1
Yakut, K. & Eggleton, P. P. 2005, ApJ, 629, 1055, https://doi.org/10.1086/431300
Zhu, L.-Y., Zhao, E.-G., & Zhou, X. 2016, RAA, 16, 68, https://doi.org/10.1088/1674/4527/16/4/068

H. Aceves & R. Michel: Instituto de Astronomia, UNAM. A.P. 877, 22800 Ensenada, BC, México (aceves, rmm@astro.unam.mx).
A. Bulut: Department of Physics, Faculty of Science, University of Çanakkale Onsekiz Mart, Terzioglu Campus, TR-17020, Çanakkale, Türkiye.
A. Bulut: Astrophysics Research Centre and Observatory, University of Çanakkale Onsekiz Mart, Terzioglu Campus, TR-17020, Çanakkale, Türkiye.
A. Keskin & M. Tanriver: Department of Astronomy and Space Science, Faculty of Science, University of Erciyes, TR-38039, Kayseri, Türkiye (mtanriver@erciyes.edu.tr).
M. Tanriver: Astronomy and Space Science Observatory Application and Research Center, University of Erciyes, TR-38039, Kayseri, Türkiye.